Articles

Contribution of the Hydrogen-Bond Network Involving a Tyrosine Triad in the Active Site to the Structure and Function of a Highly Proficient Ketosteroid Isomerase from *Pseudomonas putida* Biotype B[†,‡]

Do-Hyung Kim, Do Soo Jang, Gyu Hyun Nam, Gildon Choi, Jeong-Sun Kim, Nam-Chul Ha, Min-Sung Kim, Byung-Ha Oh, and Kwan Yong Choi*

Division of Molecular Life Sciences and Center for Biofunctional Molecules, Pohang University of Science and Technology, Pohang 790-784, South Korea

Received September 9, 1999; Revised Manuscript Received December 23, 1999

ABSTRACT: Δ^5-3-Ketosteroid isomerase from *Pseudomonas putida* biotype B is one of the most proficient enzymes catalyzing an allylic isomerization reaction at rates comparable to the diffusion limit. The hydrogen-bond network (Asp99···Wat504···Tyr14···Tyr55···Tyr30) which links the two catalytic residues, Tyr14 and Asp99, to Tyr30, Tyr55, and a water molecule in the highly apolar active site has been characterized in an effort to identify its roles in function and stability. The $\Delta G_U^{H_2O}$ determined from equilibrium unfolding experiments reveals that the elimination of the hydroxyl group of Tyr14 or Tyr55 or the replacement of Asp99 with leucine results in a loss of conformational stability of 3.5−4.4 kcal/mol, suggesting that the hydrogen bonds of Tyr14, Tyr55, and Asp99 contribute significantly to stability. While decreasing the stability by about 6.5−7.9 kcal/mol, the Y55F/D99L or Y30F/D99L double mutation also reduced activity significantly, exhibiting a synergistic effect on k_{cat} relative to the respective single mutations. These results indicate that the hydrogen-bond network is important for both stability and function. Additionally, they suggest that Tyr14 cannot function efficiently alone without additional support from the hydrogen bonds of Tyr55 and Asp99. The crystal structure of Y55F as determined at 1.9 Å resolution shows that Tyr14 OH undergoes an alteration in orientation to form a new hydrogen bond with Tyr30. This observation supports the role of Tyr55 OH in positioning Tyr14 properly to optimize the hydrogen bond between Tyr14 and C3-O of the steroid substrate. No significant structural changes were observed in the crystal structures of Y30F and Y30F/Y55F, which allowed us to estimate approximately the interaction energies mediated by the hydrogen bonds Tyr30···Tyr55 and Tyr14···Tyr55. Taken together, our results demonstrate that the hydrogen-bond network provides the structural support that is needed for the enzyme to maintain the active-site geometry optimized for both function and stability.

A central question in structure−function relationship of proteins is how proteins perform their function with a given structural geometry. It is generally accepted that proteins have evolved to optimize their function rather than stability in a given environment (*1*, *2*). This stability−function relationship implies the possibility of proteins improving stability with a compromise of function. In this regard, highly proficient enzymes might help us gain insights into how the functionally optimized active-site geometry has evolved in conjunction with the overall structural stability.

One of the most proficient enzymes, Δ^5-3-ketosteroid isomerase (KSI),[1] provides a unique and highly optimized active site environment and geometry. KSI is an enzyme catalyzing the allylic rearrangement of a variety of Δ^5-3-ketosteroids to Δ^4-3-ketosteroids, shifting a double bond from the 5(6)-position to the 4(5)-position, as illustrated in Figure 1A (*3*). KSI enhances the turnover rate by more than 10^{10}-fold compared to the rate of the corresponding uncatalyzed reaction (*4*). Two enzymes from different bacterial species, *Pseudomonas putida* and *Commamonas testosteroni* (formerly known as *Pseudomonas testosteroni*), have been most intensively studied. *C. testosteroni* KSI (TI) is a homodimeric

[†] This work was supported by a grant from Korea Science and Engineering Foundation, by the Academic Research Fund of Korea Ministry of Education, and partly by the Research Center for New Biomaterials in Agriculture, Seoul National University in Korea.

[‡] The atomic coordinates of the Y30F, Y55F, and Y30F/Y55F mutants have been deposited under entry codes 1DMQ, 1DMM, and 1DMN, respectively, at the Brookheaven Protein Data Bank.

* To whom correspondence should be addressed. Telephone: 82-562-279-2295. Fax: 82-562-279-2199. E-mail: kchoi@postech.ac.kr.

[1] Abbreviations: KSI, ketosteroid isomerase; PI, KSI of *P. putida* biotype B; TI, KSI of *C. testosteroni*; 5-AND, 5-androstene-3,17-dione; WT, wild-type KSI from *P. putida*; EDTA, ethylenediaminetetraacetic acid; DTT, dithiothreitol; pSK(−), pBluescript SK(−); SDS−PAGE, sodium dodecyl sulfate−polyacrylamide gel electrophoresis; CD, circular dichroism; $\Delta G_U^{H_2O}$, Gibbs free-energy change for unfolding in the absence of urea and at 25 °C.

10.1021/bi992119u CCC: $19.00
Published on Web 03/28/2000

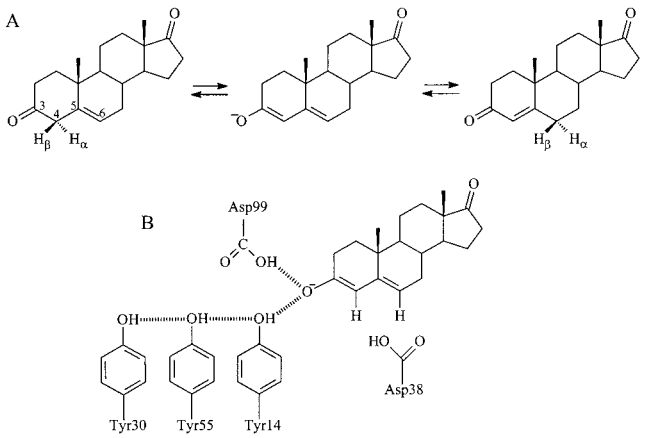

FIGURE 1: (A) Scheme of the allylic isomerization reaction catalyzed by KSI. (B) Schematic diagram illustrating the H-bond network connecting Asp99 to the tyrosine triad of Tyr14, Tyr30, and Tyr55 via C3-O of the dienolate reaction intermediate.

enzyme with 125 amino acids in each monomer (*5*). The *P. putida* (PI) is six residues longer than TI, and its amino acid sequence is 34% identical with that of TI (*6*). The catalytic mechanism of KSI is known to proceed via a dienolate intermediate by the concerted action of Tyr14 and Asp38 (numbered according to the TI sequence throughout the text) (*7*, *8*). Tyr14 plays a crucial role in catalysis by donating a hydrogen bond directly to C3-O of the dienolate intermediate (*9*), while Asp99 is also implicated in hydrogen bonding either to C3-O of the intermediate (*10*, *11*) (Figure 1B) or to Tyr14 (*12*). With regard to the catalytic roles of Tyr14 and Asp99, there are still controversies over the existence and contribution of the low-barrier hydrogen bond proposed to be present between Tyr14 Oη and C3-O of the dienolate intermediate (*10*, *13*−*15*) or between Asp99 Oδ2 and Tyr14 Oη (*12*, *16*, *17*).

Three-dimensional structures of both KSI enzymes determined recently by X-ray crystallography (*10*, *15*) and by NMR spectroscopy (*11*) reveal that this small protein is folded into a six-stranded β-sheet and three α-helices in each monomer. The active site comprises a conical cleft 14−16 Å deep. Most of the active-site cleft of KSI is hydrophobic in nature, to be effective for substrate binding. One of the most noticeable features of the KSI active-site geometry is that the polar functional groups are maintained in the highly apolar active site by forming a hydrogen-bond network. The carboxyl group of the catalytic residue Asp99 is connected to the hydroxyl group of Tyr14 via a water molecule, Wat504, and in turn Tyr14 is linked to the hydrogen bond Tyr55···Tyr30, forming a H-bond network, Asp99···Wat504···Tyr14···Tyr55···Tyr30, in the crystal structure of PI (Figure 1B). This network of interactions among the active-site residues is also conserved in TI except for the replacement of Tyr30 with phenylalanine.

H-Bond networks are not rare in biological systems. As reported by Barlow and Thorton (*18*), 37% of ion pairs in protein crystal structures exist as charge networks. A number of studies have suggested that H-bond networks are important for stability as well as for catalysis (*19*−*21*). In cytochrome *c*, a H-bond network is associated with a fixed water and maintains the spatial relationships between nearby side chains, ensuring the proper orientation of the side chains in forming a hydrogen-bond interaction with the heme ligand (*19*). H-Bond networks can also contribute to catalysis by stabilizing the transition state as shown in carboxypeptidase Y (*22*). In most serine proteases, the carboxylate group of Asp102 in the catalytic triad is hydrogen bonded to Ser214, which is in turn linked to water molecules (*23*−*25*). This H-bond network was proposed to help polarize or stabilize the buried Asp102 carboxylate group, which will ultimately facilitate the catalysis (*26*, *27*). H-Bond networks are also important for stability. A number of analyses showed that an increase in the number of hydrogen bonds is the principal determinant of the increased stability (*28*−*30*). A hydrogen-bond network in λ repressor is distinguishable in that it produces a different effect on the secondary and tertiary structural stabilities (*31*). In PI, the proximity of the two tyrosine residues, Tyr30 and Tyr55, to the catalytic residue, Tyr14, and their network of interactions with Asp99 point to potential contributions of the H-bond network to catalysis. The location of the H-bond network in the highly apolar active site of PI is also expected to make a significant contribution to the stability of this protein. The study on the roles of the H-bond network of KSI in catalysis and stability will be valuable for understanding the design principle of the active-site geometry of proficient enzymes.

In this study, the H-bond network of the PI active site was perturbed by replacing Tyr14, -30, and -55 with phenylalanine or Asp99 with leucine individually or in combinations. The respective mutational effects were then analyzed in terms of catalysis and stability. The energetic contribution of the interactions mediated by the H-bond network to stability was assessed using equilibrium unfolding experiments with urea denaturation. Kinetic parameters determined for the mutant enzymes exhibited a synergistic effect on k_{cat} for the Y55F/D99L and Y30F/D99L double mutations. These mutational effects on catalysis together with the crystal structure of Y55F provided insight into the roles of the H-bond network of PI in maintaining the active-site geometry to optimize the hydrogen bond between Tyr14 OH and C3-O of the steroid substrate. With the help of the crystal structures of Y30F, Y55F, and Y30F/Y55F, the proper positioning of Tyr14 was found to be important for efficient catalysis and the interaction energies mediated by the hydrogen bonds, Tyr30···Tyr55 and Tyr14···Tyr55, were approximately estimated.

EXPERIMENTAL PROCEDURES

Materials. Ultragrade urea was obtained from Sigma. 5-Androstene-3,17-dione (5-AND) was purchased from Steraloids. T4 DNA ligase, *Eco*RI, *Eco*RV, *Hin*dIII, *Cla*I, and *Apal*I were obtained from Boehringer Maennhaim. Oligonucleotides were obtained from Bioneer Inc. The Superose 12 gel filtration column and radiochemicals for sequencing were purchased from Amersham Pharmacia Biotech. Other chemicals were molecular biology grade and obtained from Sigma.

Site-Directed Mutagenesis. The tyrosine residues at positions 14, 30, and 55 of PI were replaced individually with Phe to make Y14F, Y30F, and Y55F according to the procedure described previously (*32*); single-stranded uracil-containing template DNA complementary to the coding strand of the isomerase gene was obtained from pSW2 (*33*), a pBluescript SK(−) [pSK(−)] plasmid containing the PI

gene, which had been introduced in *Escherichia coli* RZ1032 after infection with the helper phage M13K07 (Pharmacia). Oligonucleotides 5′-TGG CCC GTT TCA TCG AGC T-3′, 5′-GAT ATC GAG GCG ATT GTG CAG ATG TTC GCC GAT GAC G-3′, and 5′-CAG ATT GCC GCG TTC TTT CGG CAG GGT T-3′ were synthesized for the preparations of Y14F, Y30F, and Y55F, respectively, and used as primers for the respective mutagenesis; the underlined nucleotides represent those changed for the point mutations. The mutated gene in pSK(−) was digested with *Eco*RI and *Hin*dIII to isolate the inserted DNA fragment and then subcloned into *Eco*RI and *Hin*dIII sites of pKK223-3 (Pharmacia). The Y30F/Y55F double point mutation was prepared by site-directed mutagenesis using the two corresponding primers. The single mutant D99L and the Y55F/D99L double mutant were prepared by mutagenesis using the single-stranded DNA of the wild type and Y55F, respectively, as a template and 5′-CTG GAT GTC ATC CTT GTG ATG CGC-3′ as a primer. The mutation was selected by digestion with *Cla*I. The Y30F/D99L double mutant was prepared by ligation of the DNA fragment containing the Y30F mutation into *Eco*RI and *Apa*lI sites of the pKK-KSI containing the D99L mutation. All the mutations were confirmed by nucleotide sequencing of the entire gene encoding the isomerase. The mutant enzymes as well as the wild-type enzyme were produced in *E. coli* BL21DE3(pLysS) and purified to homogeneity by deoxycholate affinity chromatography and Superose 12 gel filtration chromatography according to the procedure described previously (*6*).

Determination of the Protein Concentration. The protein concentration was determined by utilizing the excitation coefficients at 280 nm of tryptophan ($\epsilon = 5500$ M^{-1} cm^{-1}) and tyrosine ($\epsilon = 1490$ M^{-1} cm^{-1}) present in the protein (*34*). The ϵ value was 16 960 M^{-1} cm^{-1} for the wild type. The accuracy of the protein concentrations was confirmed by the quantitative analysis of the bands on SDS−PAGE by use of an imaging densitometer (Bio-Rad GS-700) and the program Molecular Analyst/PC (Bio-Rad Windows software).

Solvent Accessible Area. The solvent accessible area was calculated from the X-ray coordinates by using the program Molecular Surface (*35*) supplied in Quanta software version 2 (Molecular Simulations Inc.). The probe radius for the calculation was 1.4 Å.

Circular Dichroism Measurements. Circular dichroism (CD) spectra of the enzymes were obtained by using a spectropolarimeter (Jasco 715) equipped with a Peltier-type temperature controller (Jasco model PTC-348WI). A cuvette with a path length of 1 mm was used for all spectral measurements. The wild-type or mutant enzyme at a concentration of 15 μM was preincubated for several minutes at 25 °C in a buffer containing 25 mM sodium phosphate (pH 7.0), 0.5 mM EDTA, and 1 mM dithiothreitol before the measurement. Scans were collected at 1 nm intervals with a bandwidth of 1 nm and accumulated 10 times. Each spectrum was corrected by subtracting the spectrum of the solution containing the used buffer and smoothed by using a program provided in the computer software of the spectropolarimeter.

Equilibrium Unfolding. The wild-type or mutant enzyme was dissolved in a buffer containing 25 mM sodium phosphate (pH 7.0), 0.5 mM EDTA, 1 mM dithiothreitol, and urea at various concentrations from 0 to 8 M. After incubation at 25 °C for more than 48 h, the mean residue molar ellipticity at 222 nm was obtained at the respective urea concentration. There was little change in the CD spectra observed after incubation for more than 48 h. The protein concentration for the measurement was 15 μM. The equilibrium constant (K_U) and free-energy change (ΔG_U) for the denaturation were determined according to a two-state model of denaturation by using the following equations (*36*):

$$F_U = (E_N - E)/(E_N - E_U) \quad (1)$$

$$K_U = 2P_T[F_U{}^2/(1 - F_U)] \quad (2)$$

$$\Delta G_U = -RT \ln(K_U) = \Delta G_U{}^{H_2O} - m[\text{urea}] \quad (3)$$

where F_U is the fraction of unfolded protein, E represents the molar ellipticity at 222 nm at a respective urea concentration, E_N and E_U are the corresponding values for the fully folded and unfolded states, respectively, and P_T is the total protein concentration. The $\Delta G_U{}^{H_2O}$ value is the free-energy change in the absence of urea, and m represents a measure of the ΔG_U dependence on urea concentration. The data from a urea denaturation curve were fitted to eq 4 (*37*) by nonlinear least-squares analysis using a graphics program, Kaleidagraph version 2.6 (Abelbeck Software).

$$E = E_N - (E_N - E_U)\exp[(m[\text{urea}] - \Delta G_U{}^{H_2O})/RT](\{1 + 8P_T/\exp[(m[\text{urea}] - \Delta G_U{}^{H_2O})/RT]\}^{1/2} - 1)/4P_T \quad (4)$$

The difference in the free-energy change for unfolding, $\Delta\Delta G_U$, between wild-type and mutant proteins was obtained with the following equation:

$$\Delta\Delta G_U = \Delta G_U - \Delta G_U{}^m \quad (5)$$

where ΔG_U and $\Delta G_U{}^m$ are the free-energy changes for unfolding of the wild-type and mutant enzymes, respectively.

Activity Assay. The catalytic activities of wild-type and mutant enzymes were determined using 5-AND as a substrate spectrophotometrically with a UV−visible spectrophotometer (Cary 3E) in the quartz cuvette with a 1.0 cm light path. Enzymatic reactions were carried out at 25 °C in the assay buffer containing 34 mM potassium phosphate (pH 7.0) and 2.5 mM EDTA with various amounts of the substrate. The final concentrations of 5-AND were 12, 35, 58, 82, and 116 μM. The final concentration of methanol was 3.3 vol %. The reaction was stopped within 1 or 2 min after the initiation of the reaction to obtain the initial reaction rate. The increase in absorbance at 248 nm was monitored with time (*6*).

Crystallization and Structure Determination. The crystals of Y30F, Y55F, and Y30F/Y55F were grown in the solution containing 1.0 M sodium acetate and 0.1 M ammonium acetate (pH 4.6) by the hanging drop method of vapor diffusion at 22 °C. The diffraction data were measured on a DIP2020 area detector with graphite-monochromated Cu Kα X-rays generated by a MacScience M18XHF rotating anode generator operated at 90 mA and 50 kV at room temperature. Data reduction, merging, and scaling were accomplished with the programs DENZO and SCALEPACK (*38*). The structure was determined by the molecular replacement program EPMR using the highly refined monomeric model of the

Table 1: Distances between the Catalytic Residues and the Nearby Atoms

Distances (Å) between the Pairs of Residues[a]			
Tyr14−Tyr30	Tyr14−Tyr55	Tyr30−Tyr55	Tyr14−Asp99
4.1 (Oη−Oη)	2.6 (Oη−Oη)	2.7 (Oη−Oη)	3.9 (Cϵ2−Oδ2)
4.2 (Cϵ1−Oϵ1)	4.2 (Cϵ1−Cξ)	3.9 (Cϵ1−Cϵ1)	4.4 (Oη−Oδ2)
4.4 (Cϵ1−Cξ)	4.3 (Cξ−Cξ)	4.1 (Cϵ1−Cξ)	4.5 (Cξ−Oδ2)
4.7 (Cδ1−Cϵ1)	4.4 (Cξ−Cϵ2)	4.2 (Cξ−Cϵ1)	4.7 (Cδ2−Oδ2)
Atoms within 5 Å of the Oxygen Atom[b]			
Tyr14 Oη	Tyr30 Oη	Tyr55 Oη	Asp99 Oδ2
Val18 Cγ2 (4.0)	Val36 Cγ2 (3.8)	Met112 Cϵ (3.9)	Phe82 Cϵ2 (3.3)
Met112 Cϵ (4.1)	Met112 Cγ (3.8)	Phe54 Cϵ2 (4.2)	Phe82 Cξ (3.3)
Met101 Cϵ (4.5)	Met112 Cγ (3.9)	Phe54 Cϵ2 (4.3)	Met84 Cϵ (3.7)
Ile26 Cγ2 (4.9)	Met112 Cϵ (4.2)	Ile26 Cγ2 (4.6)	Met112 Cϵ (4.0)
	Met101 Cϵ (4.4)	Val36 Cγ2 (4.9)	Met101 Cϵ (4.2)
	Met112 Sδ (4.6)		Met112 Sδ (4.7)
	Ile109 Cδ1 (4.6)		
	Ile109 Cγ2 (4.8)		

[a] The four shortest distances are listed with the corresponding atoms in parentheses. [b] Atoms found within 5 Å of the respective oxygen atom of the three tyrosine residues and Asp99. The atoms belonging to Tyr14, Tyr30, Tyr55, and Asp99 are excluded since they are already listed in part a. The number in parentheses represents the distance (Å) between the corresponding atoms.

uninhibited PI. Further refinement was carried out with X-PLOR (*39*).

RESULTS

Geometry of the H-Bond Network. The examination of the crystal structure of PI reveals that the tyrosines at positions 14, 30, and 55 are located at the bottom of the highly apolar active site pocket where they form the H-bond network, Tyr30···Tyr55···Tyr14. Tyr14 and Tyr55 are located on α-helices A1 and A3, respectively, while Tyr30 is located on the loop connecting α-helix A2 and β-strand B1. The distances between the oxygen atoms in the OH groups of these tyrosine residues are 2.6 Å for Tyr14 Oη and Tyr55 Oη and 2.7 Å for Tyr55 Oη and Tyr30 Oη (Table 1).

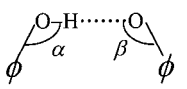

α : Angle for donor of hydrogen bond
β : Angle for acceptor of hydrogen bond
ϕ : phenyl ring

The angles of the donors and acceptors of the hydrogen bonds are in the range of 116−136°. They are very close to the ideal values, 120° and 135°, for the angles of the donor and acceptor of the hydrogen bonds, respectively, mediated by Oη's of a tyrosine residue which is classified as Osp^2 (*21*). On the other hand, Oη's of Tyr14 and Tyr30 are 4.1 Å apart which might be too far for a hydrogen bond to form. Tyr14 Oη is also bridged to Asp99 Oδ2 by Wat504. The hydroxyl groups of the tyrosine residues and the carboxyl group of Asp99 are surrounded by apolar atoms from Val18, Ile26, Val36, Phe54, Phe82, Met84, Met101, Ile109, and Met112 (Table 1). The local dielectric constant near Tyr14 in the TI active site has been estimated to be 18 ± 2 (*40*), reflecting a highly apolar active-site environment. The tyrosine triad and the functional polar groups are accommodated in the highly apolar active site by forming possible hydrogen bonds and satisfying the internal packing.

The calculation of the solvent accessible areas of the three tyrosine residues indicates that Tyr30 is completely buried while the hydroxyl group of Tyr14 and the phenyl ring moiety of Tyr55 are partially exposed to solvent with solvent accessible areas of 6 and 7 Å^2, respectively. The environment of the hydroxyl group of Tyr30 is highly apolar, surrounded by Ile26, Val36, Ile51, Met101, Ile109, Met112, and the phenyl ring moieties of Tyr14 and Tyr55 (Table 1). The complete burial of the phenyl ring moiety of Tyr14 as well as its connection to Tyr55, Wat504, and Asp99 through the H-bond network may contribute to the rigidity of Tyr14 OH. The temperature factor of Tyr14 Oη is as small as 14.1 Å^2 and becomes much smaller (9.82 Å^2) when equilenin, a reaction intermediate analogue, binds to the enzyme. The high rigidity even in the absence of the steroid would contribute to lowering entropic barriers in the enzymatic catalysis. The ^{13}C NMR relaxation studies on TI confirmed the rigidity of the Tyr14 hydroxyl group in complex with a steroid (*41*). This is consistent with the previous observation of a low-frequency motion of Tyr14 as detected with fluorescence anisotropy decay measurements (*42*).

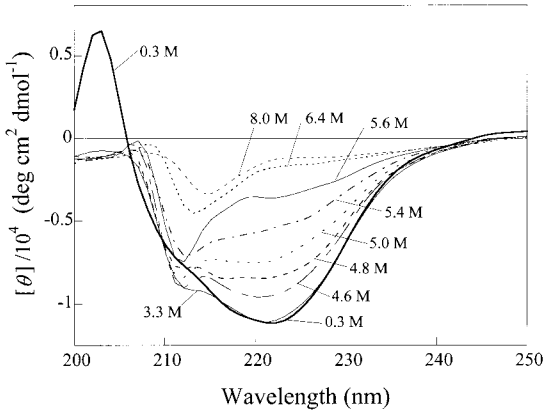

FIGURE 2: CD spectra of the WT obtained at different urea concentrations. The measurement was carried out at a protein concentration of 15 μM in the buffer containing 25 mM potassium phosphate, 0.5 mM EDTA, 1 mM DTT at pH 7.0, and urea at the indicated concentrations. The spectra were obtained after incubation of the enzyme with urea for 48 h, by which the enzyme reached the equilibrium state.

Preparation of Mutant Enzymes. To investigate how much the H-bond network in the active site of PI contributes to catalysis and conformational stability, the tyrosine residues and Asp99 were replaced with phenylalanine and leucine, respectively, to generate Y14F, Y30F, Y55F, Y30F/Y55F, Y30F/D99L, and Y55F/D99L. The mutant enzymes were successfully overexpressed in soluble forms as highly as the wild-type enzyme (WT) and bound specifically to the deoxycholate affinity resin. The purified proteins were homogeneous as judged by SDS−PAGE analysis (data not shown). The mutant enzymes exhibited protein bands of an identical size on SDS−PAGE corresponding to a molecular mass of about 14 kDa for the monomer. The expression levels were similar to that of the WT with a yield of about 10 mg per 200 mL of culture.

Effects of Mutations on Conformational Stability. The CD spectrum of the WT in the far-UV region exhibited a broad negative maximum around 222 nm and a strong positive maximum near 197 nm with a shoulder peak around 208 nm, which is a typical pattern of α- or α/β-proteins (*43*) (Figure 2). The CD spectra in the far-UV region did not exhibit any gross difference between wild-type and mutant enzymes, suggesting that the mutations do not perturb the

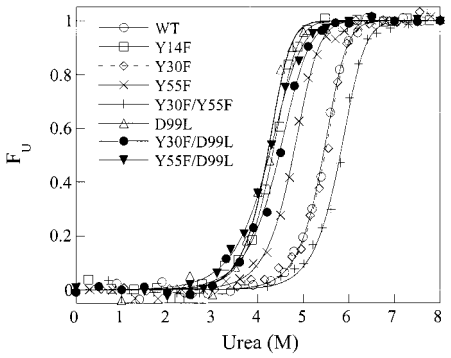

FIGURE 3: Unfolding equilibrium transition of the WT and the mutant enzymes induced by urea. The change in molecular ellipticity at 222 nm was measured, and data points were fitted to eq 4 to obtain the transition curve, which gave us the $\Delta G_U^{H_2O}$ and *m* values listed in Table 2.

secondary structure of the native KSI (data not shown). The unfolding free-energy change, ΔG_U, was determined by monitoring the CD ellipticity at 222 nm as a function of the urea concentration at 25 °C. As shown in Figure 2, the negative ellipticity near 222 nm decreased gradually with increasing urea concentrations. At high urea concentrations, the signal at 222 nm was reduced while the negative maximum near 212 nm became prominent to give the typical spectral pattern of random coil structures. When the urea concentration was increased up to 3.3 M, the signal at 222 nm did not change significantly but the content of random coil was slightly increased. Drastic changes in the spectral pattern were observed between 4 and 6 M urea. Above 6 M urea, the CD spectrum was not changed significantly, consistently exhibiting a typical pattern of a random coil structure. The transition curves were normalized by assuming that ellipticities for the native and unfolded states can be extrapolated linearly into the transition zone and nicely fitted to a two-state model (Figure 3). The values of $\Delta G_U^{H_2O}$, *m*, and $\Delta\Delta G_U$ for the wild-type and mutant enzymes were obtained according to eqs 3−5 and are given in Table 2. The transition midpoint for the KSI unfolding curve was lowest for Y55F/D99L and highest for Y30F/Y55F.

The removal of the hydroxyl group from Tyr14, Tyr55, or Asp99 decreased $\Delta G_U^{H_2O}$ by 4.4, 3.5, or 3.5 kcal/mol, respectively, relative to that of the WT, suggesting that the catalytic residues, Tyr14 and Asp99, are important for stability as well as for catalysis and Tyr55 is important for stability. The most severely destabilizing substitution was Y55F/D99L, which decreased $\Delta G_U^{H_2O}$ by 7.9 kcal/mol relative to that of the WT. The Y30F/D99L double mutation also decreased $\Delta G_U^{H_2O}$ significantly by 6.5 kcal/mol. To obtain a more realistic estimate of the contribution of the hydrogen bonds to stability, the mutational effects on both hydrophobicity and side-chain conformational entropy were incorporated in the calculation of $\Delta\Delta G_U$ (*44*) (Table 2). The corrected $\Delta\Delta G_U$ was higher than the measured $\Delta\Delta G_U$ by 1.5−5 kcal/mol. The higher values of the corrected $\Delta\Delta G_U$ are due to the energetically favorable locations of phenylalanine and leucine in the interior of proteins instead of tyrosine and aspartate, respectively. The simultaneous elimination of two completely buried hydroxyl groups from Tyr30 and Tyr55 as well as the elimination of the hydroxyl group from Tyr30 decreased $\Delta G_U^{H_2O}$ by 3.3 and 1.6 kcal/mol, respectively, relative to that of the WT. These results suggest

Table 2: Changes in the Free Energies of Unfolding of Wild-Type and Mutant KSI Determined by Reversible Denaturation with Urea[a,b]

enzyme	$\Delta G_U^{H_2O}$ [c]	*m*[d]	$[\text{urea}]_{50\%}$[e]	$\Delta\Delta G_U$ (kcal/mol) measured[f]	$\Delta\Delta G_U$ (kcal/mol) corrected[g]	$\Delta\Delta G_U$/HB[h]
wild-type	24.3	3.39	5.22	–	–	–
Y14F	19.9	3.10	4.30	4.4	5.9	3.0
Y30F	24.3	3.23	5.49	0	1.6	1.6
Y55F	20.8	2.98	4.77	3.5	5.1	5.1
Y30F/Y55F	24.3	3.05	5.81	0	3.3	1.7
D99L	20.5	3.32	4.19	3.8	7.2	3.6
Y30F/D99L	17.8	2.52	4.45	6.5	11.5	3.8
Y55F/D99L	16.4	2.31	4.25	7.9	12.9	4.3

[a] Measurements were performed at 25 °C and pH 7.0. Values were obtained from fits to the data from Figure 3 according to eq 4. [b] Standard errors are 5−10%. [c] $\Delta G_U^{H_2O}$ (kilocalories per mole) represents the free-energy change in the absence of urea. [d] *m* (kilocalories per mole per molar) is the slope of the linear denaturation plot, $d\Delta G_U/d[\text{urea}]$. [e] $[\text{urea}]_{50\%}$ (molar) is the concentration of urea at which 50% of the protein is unfolded. It was obtained from the relationship $[\text{urea}]_{50\%} = [(RT \ln P_T) + \Delta G_U^{H_2O}]/m$. [f] Values obtained from eq 5. [g] The corrected $\Delta\Delta G$ values = [measured values + (fraction polar group buried)(difference in hydrophobicity) − (difference in $T\Delta S_{conf}$)]. The differences in hydrophobicity and $T\Delta S_{conf}$ are 1.13 and −0.51 kcal/mol for the Tyr → Phe mutation and 3.37 and −0.07 kcal/mol for the Asp → Leu mutation, respectively, which are based on the *n*-octanol hydrophobicity scale of Flauchere and Pliska (*45*) and on the mean $T\Delta S_{conf}$ values at 300 K given by Doig and Sternberg (*46*), respectively. The fraction polar group buried was determined using the method of Lee and Richards (*35*), as implemeneted by Lesser and Rose (*47*). [h] The values are per hydrogen bond. The number of hydrogen bonds removed was assumed to be two for Y14F and D99L and three for Y30F/D99L and Y55F/D99L, while the number was determined to be one for Y30F and Y55F and two for Y30F/Y55F on the basis of their crystal structures (Figure 4).

that all of the hydrogen bonds forming the network are important for protein stability. By dividing the corrected $\Delta\Delta G_U$ by the number of hydrogen bonds removed by the mutations, we estimated that the removed hydrogen bond contributes an average of 3.3 kcal/mol per hydrogen bond to stability.

Effects of Mutations on Catalysis. To understand the roles of the H-bond network in catalysis, the k_{cat} and K_m values of the mutant enzymes were determined using 5-AND as a substrate. The Y55F mutation decreased k_{cat} by about 6-fold, suggesting that the H-bond network of the tyrosine triad, Tyr30···Tyr55···Tyr14, contributes about 1.1 kcal/mol to catalysis (Table 3). Interestingly enough, k_{cat} was significantly decreased by about 18000-fold for Y55F/D99L, which is ∼3000 and ∼180 times higher in effect than the Y55F and D99L single mutations, respectively, and even ∼11 times higher in effect than the Y14F mutation. The cooperative effect of the double mutation indicates that the OH of Tyr14 alone cannot play the catalytic role efficiently when not assisted by the hydrogen bond from either Tyr55 or Asp99. Another possibility is that the replacement of Asp99 with leucine will introduce a steric hindrance in the active site affecting the geometry of Tyr14 OH, which could have a more drastic effect on k_{cat} when the hydroxyl group of Tyr55 is additionally eliminated. k_{cat} was also decreased synergistically by about 520-fold for Y30F/D99L relative to that of the WT. This result indicates that the Y30F mutation might affect somehow the catalytic role of Tyr14 that is linked to Tyr30 by the H-bond network. Interestingly, the Y30F/Y55F double mutation restored the catalytic activity up to half of

Table 3: Kinetic Parameters of Wild-Type and Mutant KSI toward 5-AND[a]

enzyme	k_{cat} (s^{-1})	K_m (μM)	k_{cat}/K_m (M^{-1} s^{-1})	relative[b] k_{cat}	relative[b] K_m
WT[c]	21230 ± 810	49.9 ± 1.3	$(4.3 \pm 0.2) \times 10^8$	1.00	1.00
Y14F[d]	13.3 ± 0.6	17.1 ± 3.1	$(7.8 \pm 0.4) \times 10^5$	$10^{-3.2}$	0.34
Y30F	17800 ± 70	55.2 ± 2.0	$(3.3 \pm 0.1) \times 10^8$	0.84	1.11
Y55F	3510 ± 60	23.0 ± 1.0	$(1.5 \pm 0.3) \times 10^8$	0.17	0.46
Y30F/Y55F	10680 ± 350	50.2 ± 5.5	$(2.1 \pm 0.1) \times 10^8$	0.50	1.01
D99L	220 ± 9	25.8 ± 0.8	$(8.5 \pm 0.3) \times 10^6$	$10^{-2.0}$	0.52
Y30F/D99L	40.7 ± 1.4	73.5 ± 11.8	$(5.5 \pm 0.2) \times 10^5$	$10^{-2.7}$	1.47
Y55F/D99L	1.2 ± 0.4	61.9 ± 6.2	$(1.9 \pm 0.6) \times 10^4$	$10^{-4.2}$	1.24

[a] The assays were performed at 25 °C in the buffer containing 34 mM potassium phosphate (pH 7.0), 2.5 mM EDTA, and 3.3% methanol. The values were obtained from three or five separate determinations. [b] Values relative to those of the WT. [c] Values from Kim et al. (*48*). [d] Values from Kim and Choi (*33*).

Table 4: Data Collection and Refinement Statistics for the Crystal Structure of the Wild-Type and Mutant Enzymes

	PI[a]	TI[b]	Y30F	Y55F	Y30F/Y55F
space group	*C*2221	*P*6522	*C*2221	*C*2221	*C*2221
unit cell [*a*, *b*, *c* (Å); α, β, γ (deg)]	36.40, 96.12, 74.40; 90.0, 90.0, 90.0	61.68, 61.68, 143.60; 90.0, 90.0, 120.0	36.37, 95.74, 74.25; 90.0, 90.0, 90.0	36.09, 95.98, 74.25; 90.0, 90.0, 90.0	36.36, 96.48, 74.60; 90.0, 90.0, 90.0
resolution (Å)	1.9	2.3	2.15	1.9	2.05
R_{sym}[c]	0.061	0.036	0.053	0.046	0.066
completeness ($F > 1\sigma$) (%)	96.2	95	91.7	93.5	93.3
R factor[d] (%)	19.8	20.5	18.2	18.9	19.5
rmsd[e] from ideal					
bond lengths (Å)	0.010	0.012	0.011	0.013	0.019
bond angles (deg)	1.590	1.615	1.592	1.548	2.03
no. of water molecules	37	29	37	37	48
average *B* factor (Å^2) for protein atoms	27.0	20.5	21.0	20.0	25.2

[a] Kim et al. (*10*). [b] Cho et al. (*15*). [c] $R_{sym} = \Sigma|I_{obs} - I_{avg}|/\Sigma I_{obs}$, where I_{obs} is an individual intensity measurement and I_{avg} is the average intensity for this reflection summed over all the data. [d] *R* factor $= \Sigma||F_o| - |F_c||/\Sigma|F_o|$. [e] Root-mean-square deviation from ideal values.

the level of the WT, which is about 3 times higher in activity than that of Y55F. K_m was decreased by about 2.9-, 2.2-, and 1.9-fold for Y14F, Y55F, and D99L, respectively, while it was marginally changed for Y30F, Y30F/Y55F, Y30F/D99L, and Y55F/D99L. The cause of the decrease in K_m is hard to address, but it might result from either an increase in affinity for the substrate or a decrease in the rate constant for the conversion of the substrate to the reaction intermediate.

Determination of the Crystal Structures of Y30F, Y55F, and Y30F/Y55F Mutant Enzymes. To understand the observed stability and catalytic activity of the tyrosine mutant enzymes on a structural basis, the crystal structures of Y30F, Y55F, and Y30F/Y55F were determined at resolutions of 2.15, 1.9, and 2.05 Å, respectively (Table 4). The overall structure was not changed by the mutations. In contrast to negligible positional rearrangements of the active-site residues observed for Y30F (Figure 4A), a closer examination of the Y55F structure around the site of the mutation reveals that the phenyl ring of Tyr14 turns toward Phe55 by 13.7° (Figure 4B). This movement results in the positional shift of Wat504 and Tyr14 Oη by 1.09 and 0.72 Å, respectively. Although the average lengths of the hydrogen bonds, Tyr14···Wat504 and Asp99···Wat504, are 0.21 Å longer in Y55F than those in the WT, the H-bond network, Tyr14···Wat504···Asp99, is still maintained. Interestingly, Tyr14 Oη is within hydrogen-bonding distance of Tyr30 Oη (3.02 Å apart), suggesting that a new hydrogen bond might form between Tyr14 and Tyr30. The crystal structure of Y30F/Y55F reveals that the additional Y30F mutation in Y55F reorients Tyr14 to the position occupied originally in the WT (Figure 4C). The distances between the catalytic residues as well as the temperature factors in Y30F/Y55F are very similar to those in the WT.

DISCUSSION

Contribution of the H-Bond Network to Stability. The significant decrease in stability produced by the Y14F mutation suggests that the catalytic residue Tyr14 is important for both stability and function. The elimination of the OH group from Tyr14 may liberate Wat504 that is located in a position between Tyr14 and Asp99. However, Asp99 may remain hydrated and Tyr55 may maintain the hydrogen bond with Tyr30 since the mutation does not cause any significant structural perturbation. Hence, $\Delta\Delta G_U^{H_2O}$ would reflect the cost of removing the two hydrogen bonds, Tyr14···Wat504 and Tyr14···Tyr55. Removal of the hydroxyl group of Tyr55 eliminates two hydrogen bonds, Tyr30···Tyr55 and Tyr14···Tyr55, but results in a noticeable change in the active-site geometry with the inclination of the phenyl ring of Tyr14 toward Tyr30, thus generating a new hydrogen bond with Tyr30 (Figure 4B). This structural rearrangement is consistent with the tendency of the polar groups in interior of proteins to make hydrogen bonds with nearby polar groups contributing to the global structural stability. This alteration in the geometry of Tyr14 also leads to changes in the strength of the Tyr14···Wat504 and Wat504···Asp99 hydrogen bonds, whose lengths increase by about 0.21 Å as shown in the crystal structure of Y55F.

The Y30F mutation did not change $\Delta\Delta G_U$. The crystal structure of Y30F at 2.15 Å resolution reveals that Tyr14 Oη moves about 0.1 Å away from Tyr55 Oη without causing

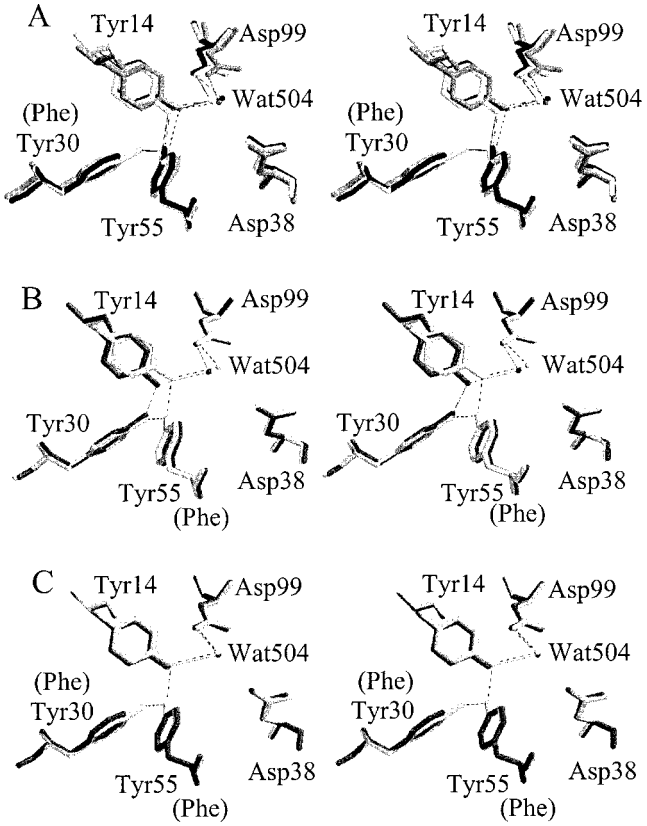

FIGURE 4: Stereoview of the active site residues of the wild-type and mutant enzymes. (A) PI (light gray), TI (dark gray), and Y30F (black) are superimposed. The equivalent atoms of all the residues were used for the superposition of the structures. The root-mean-square deviation for the active site atoms was 0.116 Å between PI and Y30F or 0.235 Å between TI and Y30F. (B) PI-WT (light gray) and Y55F (black) and (C) PI-WT (light gray) and Y30F/Y55F (black) were drawn after the superposition of the equivalent atoms of all the residues. A potential hydrogen bond is represented by the dashed line. Quanta version 2.0 (Molecular Simulations Inc.) was used for the superposition. Molscript (*49*) was used to draw the figure.

any significant perturbation of the hydrogen-bond geometry between Tyr14 and Tyr55 (Figure 4A). Considering the mutational effect on the stability of unfolded states, the difference in the noncovalent interaction energy between the folded states of wild-type and mutant enzymes, ΔG_F, can be approximately estimated from the relationship $\Delta\Delta G_U = \Delta G_F - \Delta G_{solv}$, where ΔG_{solv} is the difference in the noncovalent interaction energy between the unfolded states of wild-type and mutant enzymes (*50*, *51*). With the solvation energy difference, ΔG_{solv}, of ca. 5.35 kcal/mol (*52*) between tyrosine and phenylalanine in water, ΔG_F was estimated to be ca. 5.35 kcal/mol for Y30F. This value corresponds to the noncovalent interaction energy difference between the wild type and the Y30F mutant in the folded state. The Y30F/Y55F double mutation eliminating the two hydrogen bonds in the interior of the protein did not change $\Delta\Delta G_U$ either (Table 2). From the relationship $\Delta\Delta G_U = \Delta G_F - \Delta G_{solv}$, ΔG_F was estimated to be 10.7 kcal/mol. This value will represent the difference in the noncovalent interaction energies between the WT and Y30F/Y55F. The interaction energies mediated by the hydrogen bonds are therefore very high in the highly aploar active-site environment of PI.

The significant decrease in stability produced by the Y55F/D99L or Y30F/D99L double mutation is correlated with the

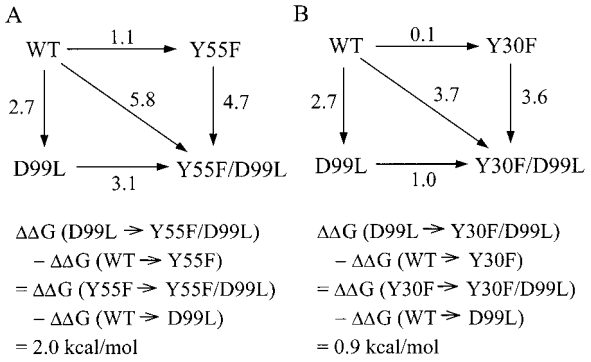

FIGURE 5: Double-mutant cycle analysis of the mutational effect on k_{cat} for two residues, Tyr55 and Asp99 (A) or Tyr30 and Asp99 (B). The value represents the free-energy difference, $\Delta\Delta G$(mutation$_I$−mutation$_{II}$), derived from the ratio of the effects of the indicated mutations on k_{cat}, which was calculated from the values listed in Table 3 with the relationship $RT \ln(k_{cat}^{mutation_I}/k_{cat}^{mutation_{II}})$. The unit of the value is kilocalories per mole.

number of the hydrogen bonds removed by the mutations. The CD spectra of Y30F/D99L and Y55F/D99L that are almost identical with that of the WT indicate that the decrease in stability by the mutations is not due to a significant structural change but to a subtle difference in the interactions between the catalytic residues. When the $\Delta\Delta G_U$/HB values for Y30F, Y55F, and D99L are being compared, it can be concluded that the hydrogen bonds linked to Wat504 contribute more to stability than the Tyr30···Tyr55 and Tyr55···Tyr14 hydrogen bonds (Table 2). The high value of $\Delta\Delta G_U$/HB for Y55F might be related to the weakening of the Tyr14···Wat504 and Wat504···Asp99 hydrogen bonds induced by the perturbation of Tyr14 in Y55F as reflected in the crystal structure of Y55F. The high value of $\Delta\Delta G_U$/HB for Y14F also supports the notion that the Tyr14···Wat504 hydrogen bond might contribute significantly to stability.

Contribution of the H-Bond Network to Catalysis. The mutational effect of Y55F on k_{cat} became more drastic when the carboxyl group of Asp99 was additionally replaced with the methyl groups of a leucine. The effect of mutations on the stabilization of the transition state was estimated by comparing the ratio of the k_{cat} values between the enzymes, and the energetic perturbation affected by mutations was evaluated on the basis of the difference in the free-energy change calculated with the equation $\Delta\Delta G = RT \ln(k_{cat}^{mutation_I}/k_{cat}^{mutation_{II}})$. The ratio of the k_{cat} values for Y55F and Y55F/D99L gives ca. 4.7 kcal/mol as the energy for the contribution of the Asp99 carboxyl group to catalysis in the absence of the hydroxyl group of Tyr55 (Figure 5). This value is about 2 kcal/mol higher than the contribution of Asp99 in the presence of Tyr55, which could be obtained from the k_{cat} values for the WT and D99L. The ratio of the k_{cat} values for D99L and Y55F/D99L gives a value of ca. 3.1 kcal/mol for the contribution of Tyr55 OH to catalysis when the carboxyl group of Asp99 was replaced with leucine. This value is also about 2 kcal/mol higher than the contribution of Tyr55 OH to catalysis in the presence of Asp99. This large deviation from simple additivity in the mutational effect may reflect the indirect interaction between Tyr55 and Asp99 through the H-bond network since large structural perturbations are not likely to be caused by the mutations as judged by the CD spectra. The synergistic effect on k_{cat} was also

observed for the Y30F/D99L double mutation relative to the respective single mutations. The energetic estimation suggests that Tyr30 OH contributes ca. 1.0 kcal/mol to catalysis when the carboxyl group of Asp99 is replaced with leucine, which is 0.9 kcal/mol higher than the value with Asp99. This result also supports the notion that Tyr30 and Asp99 interact with each other through the H-bond network.

Unfortunately, crystal structures are not available for Y30F/D99L and Y55F/D99L, which are essential for understanding the synergistic effects of the mutations. The crystal structure of Y55F reveals that the mutation moves Tyr14 OH away from the substrate-binding site, which would result in an unfavorable interaction between Tyr14 and C3-O of the steroid substrate (Figure 4B). This suggests that Tyr55 OH plays a role in positioning Tyr14 OH properly to optimize the hydrogen bond between Tyr14 and C3-O of the substrate. The additional substitution of Asp99 for Leu in Y55F will perturb the position of Wat504 O and weaken the attractive hydrogen-bond interaction between Tyr14 and Wat504 to move Tyr14 OH further away from the substrate-binding site. This positional perturbation will make the hydrogen bond between Tyr14 Oη and C3-O of the steroid more energetically unfavorable, resulting in the drastic effect of the Y55F/D99L double mutation on k_{cat}. The close relationship between the geometry of Tyr14 and the catalytic activity is also reflected in the crystal structure of Y30F/Y55F and its activity (Figure 4C and Table 3). The additional Y30F mutation in Y55F reorients the position of Tyr14 to that occupied in the WT, and the activity was consistently restored to half the level of the WT.

H-Bond Network Satisfying both Function and Stability. The active-site geometry with the tyrosine triad forming the H-bond network in PI is a rare example of how the enzyme has evolved to fulfill the function optimally with little compromise of the conformational stability. A number of enzymes are known to have catalytic groups in energetically unfavorable environments that destabilize the protein structure to promote efficient catalysis. In T4 lysozyme, mutations at four active-site residues abolished or reduced enzymatic activity but increased thermal stability by 0.7−2.0 kcal/mol (*53*). Mutations at substrate-binding residues His274 and Asp375 in citrate synthase increased stability while decreasing activity by 3−4 orders of magnitude (*54*). Similar results have been reported for several other proteins, including barnase, staphylococcal nuclease, retinoic acid-binding protein, and λ cro repressor (*55*−*62*). In such cases, mutations at the active site or substrate-binding residues increased conformational stability while reducing activity. Contrary to these examples, pancreatic ribonuclease A provides an example in which His119−Asp121 interaction contributes equally to both function and stability (*63*).

The active-site geometry of TI is very similar to that of PI, as indicated previously with a small root-mean-square difference of 0.667 Å in the superposition of the two crystal structures (*15*) (Figure 4A). In TI, the network of hydrogen bonds involving Tyr14, Tyr55, Asp99, and Wat504 is conserved but Tyr30 is replaced with phenylalanine. Interestingly, the previous mutational analysis showed that the mutations of the active site residues affect k_{cat} more drastically in TI than in PI; Y14F and D99A of TI result in 50000- and 5000-fold decreases in k_{cat}, respectively, (*8*, *11*), whereas Y14F and D99A of PI result in 2000- and 100-fold decreases in k_{cat}, respectively (*33*, *64*, *65*). Such differences might be due either to the larger compensatory roles of the remaining catalytic residues in PI or to the higher vulnerability of the active-site geometry to the perturbation by the mutations in TI. Even though Tyr30 OH does not seem to be important for catalysis, the replacement of Tyr30 with phenylalanine might be partly responsible for the greater perturbation of the active-site geometry in TI as shown in the synergistic effect of the Y30F/D99L double mutation on k_{cat}.

In conclusion, the mutational studies on the roles of the H-bond network in the active site of PI demonstrate that the H-bond network is important for both function and stability. The synergistic effect of the mutations of the catalytic residues on catalysis suggests that the roles of Tyr55 and Asp99 are important in positioning Tyr14 to optimize the hydrogen bond between Tyr14 and C3-O of the steroid substrate. The crystal structures of Y55F and Y30F/Y55F support the importance of the proper positioning of Tyr14 for efficient catalysis. The H-bond network provides the structural support for the protein to maintain the active-site geometry optimized for the function with little compromise of stability. To make it clear, the mutational effects on catalysis and stability should be reevaluated on the basis of the three-dimensional structures of all the mutant enzymes. These studies will contribute to a better understanding of the roles of the hydrogen bonds involving the catalytic residues, Tyr14 and Asp99, in the stabilizaton of the reaction intermediate.

ACKNOWLEDGMENT

We thank Dr. Byeung Doo Song at Handong University (Pohang, South Korea) and Dr. Suhng Wook Kim at Duke University (Durham, NC) for helpful comments and discussions.

REFERENCES

1. Jaenicke, R. (1991) *Biochemistry 30*, 3146−3161.
2. Lee, B., and Vasmatzis, G. (1997) *Curr. Opin. Biotechnol. 3*, 75−83.
3. Batzold, F. H., Benson, A. M., Covey, D. F., Robinson, C. H., and Talalay, P. (1976) *Adv. Enzyme Regul. 14*, 243−267.
4. Kuliopulos, A., Talalay, P., and Mildvan, A. S. (1990) *Biochemistry 29*, 10271−10280.
5. Benson, A. M., Jarabak, J., and Talalay, P. (1971) *J. Biol. Chem. 246*, 7514−7525.
6. Kim, S. W., Kim, C. Y., Benisek, W. F., and Choi, K. Y. (1994) *J. Bacteriol. 176*, 6672−6676.
7. Xue, L., Talalay, P., and Mildvan, A. S. (1990) *Biochemistry 29*, 7491−7500.
8. Kuliopulos, A., Mildvan, A. S., Shortle, D., and Talalay, P. (1989) *Biochemistry 28*, 149−159.
9. Xue, L., Talalay, P., and Milvan, A. S. (1991) *Biochemistry 30*, 10858−10865.
10. Kim, S. W., Cha, S.-S., Cho, H.-S., Kim, J.-S., Ha, N.-C., Cho, M.-J., Joo, S., Kim, K.-K., Choi, K. Y., and Oh, B.-H. (1997) *Biochemistry 36*, 14030−14036.
11. Wu, Z. R., Ebrahimian, S., Zawrotny, M. E., Thornburg, L. D., Perez-Alvarado, G. C., Brothers, P., Pollack, R. M., and Summers, M. F. (1997) *Science 276*, 415−418.
12. Massiah, M. A., Abeygunawardana, C., Gittis, A. G., and Mildvan, A. S. (1998) *Biochemistry 37*, 14701−14712.
13. Gerlt, J. A., and Gassman, P. G. (1993) *J. Am. Chem. Soc. 115*, 11552−11568.
14. Zhao, Q., Abeygunawardana, C., Talalay, P., and Milvan, A. S. (1996) *Proc. Natl. Acad. Sci. U.S.A. 93*, 8220−8224.

15. Cho, H.-S., Choi, G., Choi, K. Y., and Oh, B.-H. (1998) *Biochemistry 37*, 8325−8330.
16. Zhao, Q., Abeygunawardana, C., and Mildvan, A. S. (1997) *Biochemistry 36*, 3458−3472.
17. Zhao, Q., Abeygunawardana, C., Gittis, A. G., and Mildvan, A. S. (1997) *Biochemistry 36*, 14616−14626.
18. Barlow, D. J., and Thornton, J. M. (1983) *J. Mol. Biol. 168*, 867−885.
19. Berghuis, A. M., Guillemette, J. G., McLendon, G., Sherman, F., Smith, M., and Brayer, G. D. (1994) *J. Mol. Biol. 236*, 786−799.
20. Sekharudu, C., Ramakrishnan, B., Huang, B., Jiang, R.-T., Dupureur, C. M., Tsai, M.-D., and Sundaralingam, M. (1992) *Protein Sci. 1*, 1585−1594.
21. Stickle, D. F., Presta, L. G., Dill, K. A., and Rose, G. D. (1992) *J. Mol. Biol. 226*, 1143−1159.
22. Mortensen, U. H., Remington, J., and Breddam, K. (1994) *Biochemistry 33*, 508−517.
23. Dutler, H., and Bizzozero, S. A. (1989) *Acc. Chem. Res. 22*, 322−327.
24. Finer-Moore, J. S., Kossiakoff, A. A., Hurley, J. H., Earnest, T., and Stroud, R. M. (1992) *Proteins 12*, 203−222.
25. Meyer, E. (1992) *Protein Sci. 1*, 1543−1562.
26. Blow, D. M. (1969) Charge relay + polarization. *Nature 221*, 337−340.
27. Birktoft, J. J., and Blow, D. M. (1972) *J. Mol. Biol. 68*, 187−240.
28. Hennig, M., Darimont, B., Sterner, R., Kirschner, K., and Jansonius, J. N. (1995) *Structure 3*, 1295−1306.
29. Salminen, T., Teplyakov, A., Karikare, J., Cooperman, B. D., Lahti, R., and Goldman, A. (1996) *Protein Sci. 5*, 1014−1025.
30. Vogt, G., Woell, S., and Argos, P. (1997) *J. Mol. Biol. 269*, 631−643.
31. Marqusee, S., and Sauer, R. (1994) *Protein Sci. 3*, 2217−2225.
32. Kunkel, T. A. (1985) *Proc. Natl. Acad. Sci. U.S.A. 82*, 488−492.
33. Kim, S. W., and Choi, K. Y. (1995) *J. Bacteriol. 177*, 2602−2605.
34. Pace, C. N., Vajdos, F., Fee, L., Grimsley, G., and Gray, T. (1995) *Protein Sci. 4*, 2411−2423.
35. Richards, F. M. (1977) *Annu. Rev. Biophys. Bioeng. 6*, 151−176.
36. Bowie, J. U., and Sauer, R. T. (1989) *Biochemistry 28*, 7139−7143.
37. Mok, Y.-K., Gay, G. D. P., Butler, P. J., and Bycroft, M. (1996) *Protein Sci. 5*, 310−319.
38. Otwinowski, Z. (1993) in *Proceedings of the CCP4 Study Weekend* (Sawyer, L., et al., Eds.) pp 56−62, SERC Daresbury Laboratory, Warrington, U.K.
39. Brunger, A. T. (1992) *X-PLOR*, version 3.0, Yale University Press, New Haven, CT.
40. Li, Y.-K., Kuliopulos, A., Mildvan, A. S., and Talalay, P. (1993) *Biochemistry 32*, 1816−1824.
41. Zhao, Q., Abeygunawardana, C., and Mildvan, A. (1996) *Biochemistry 35*, 1525−1532.
42. Wu, P., Li, Y.-K., Talalay, P., and Brand, L. (1994) *Biochemistry 33*, 7415−7422.
43. Fasman, G. D. (1996) *Circular Dichroism and the Conformational Analysis of Biomolecules*, Plenum Press, New York and London.
44. Myers, J. K., and Pace, C. N. (1996) *Biophys. J. 71*, 2033−2039.
45. Flauchere, J. L., and Pliska, V. E. (1983) *Eur. J. Med. Chem. 18*, 369−375.
46. Doig, A. J., and Sternberg, J. E. (1995) *Protein Sci. 4*, 2247−2251.
47. Lesser, G. J., and Rose, G. D. (1990) *Proteins: Struct., Funct., Genet. 8*, 6−13.
48. Kim, D.-H., Nam, G. H., Jang, D. S., Choi, G., Joo, S., Kim, J.-S., Oh, B.-H., and Choi, K. Y. (1999) *Biochemistry 38*, 13810−13819.
49. Kraulis, P. J. (1991) *J. Appl. Crystallogr. 24*, 946−950.
50. Matouschek, A., Kellis, J. T., Jr., Serrano, L., and Fersht, A. R. (1989) *Nature 340*, 122−126.
51. Horovitz, A., and Fersht, A. R. (1990) *J. Mol. Biol. 214*, 613−617.
52. Radzicka, A., and Wolfenden, R. (1988) *Biochemistry 27*, 1664−1670.
53. Shoichet, B. K., Baase, W. A., Kuroki, R., and Matthews, B. W. (1995) *Proc. Natl. Acad. Sci. U.S.A. 92*, 452−456.
54. Zhi, W., Srere, P. A., and Evans, C. T. (1991) *Biochemistry 30*, 9281−9286.
55. Meiering, E. M., Serrano, L., and Fersht, A. R. (1992) *J. Mol. Biol. 225*, 585−589.
56. Poole, L. B., Loveys, D. A., Hale, S. P., and Gerlt, J. A. (1991) *Biochemistry 30*, 3621−3627.
57. Hibler, D. W., Stolowich, N. J., Reynolds, M. A., and Gerlt, J. A. (1987) *Biochemistry 26*, 6278−6286.
58. Zhang, J., Liu, Z.-P., Jones, T. A., Gierazch, L. M., and Sambrook, J. F. (1992) *Proteins 13*, 87−99.
59. Kanzaki, H., McPhie, P., and Miles, E. W. (1991) *Arch. Biochem. Biophys. 284*, 174−180.
60. Kelley, R. F., Devos, A. M., and Cleary, S. (1991) *Proteins 11*, 35−44.
61. Kimura, S., Nakamura, H., Hashimoto, T., Oobatake, M., and Kanaya, S. (1992) *J. Biol. Chem. 267*, 21535−21542.
62. Pakula, A. A., and Sauer, R. T. (1989) *Proteins 5*, 202−210.
63. Quirk, D. J., Park, C., Thompson, J. E., and Raines, R. T. (1998) *Biochemistry 37*, 17958−17964.
64. Kim, S. W., and Choi, K. Y. (1995) *Mol. Cells 5*, 354−358.
65. Kim, S. W., Joo, S., Choi, G., Cho, H.-S., Oh, B.-H., and Choi, K. Y. (1997) *J. Bacteriol. 179*, 7742−7747.

BI992119U